Journal of materials and Environmental Sciences
ISSN : 2028-2508

JMES, 2017 Volume 8, Issue 3, Page 863-869

http://www.jmaterenvironsci.com

ICMES2016. 1-3 Dec. 2016. Ouida

Catalytic activity of ferrite nanostructure monitored with infrared spectroscopy

A.-H. El Foulani[1], A. Aamouche[1*], A. Jedaa[1], M. Amjoud[2], K. Ouzaouit[3]

1 Equipe de recherche MSISM, Département de Physique, Faculté Poly disciplinaire de Safi, Université Cadi Ayyad, BP 4162, 46000 Safi, Morocco.
2 Laboratoire de la Matière Condensée et Nanostructures, Université Cadi Ayyad, Faculté des Sciences et Techniques, Guéliz, Marrakech, Morocco.
3 Centre de recherche REMINEX, Groupe Managem, *BP. 469, Marrakech Medina 40000, Morocco.*

Received 30 Dec2016,
Revised 30 Jan2017,
Accepted 31 Jan2017,

Keywords

- ✓ Ferrite
- ✓ Catalysis ;
- ✓ AFM ;
- ✓ FTIR ;
- ✓ Methane conversion ;

a.aamouche@gmail.com,
Phone : (00212) 6 75388280

ABSTRACT

$Co_{0.5}Zn_{0.5}Fe_2O_4$ ferrite nanoparticles were synthesized using a coprecipitation method at relatively moderate temperature. Sample was characterized by X-ray diffraction and scanning force microscopy. Crystallite dimensions were determined and the crystal parameters were refined by X-ray diffraction. On the other hand, Fourier Transform Infrared spectroscopy was used to study the conversion of methane present in air-methane mixture reacting with ferrite nanoparticles powder at various temperatures. The conversion rates of CH_4 into CO_2 were determined from the evolutions of CO_2 vibrational band intensities, as a function of time and temperature. It was clearly established that the synthesized powders has good catalytic behaviors at low temperatures. The optimization of conversion temperature of CH_4 over ferrite catalyst was carried out and the catalytic activity of ferrite powder as a function of reaction time was characterized.

1. Introduction

Cobalt ferrite materials have attracted a great interest in fundamental and applied research due to their thermal stability, mechanical hardness, large coercive field, high magnetostriction coefficient and anisotropy constant. All these characteristics encourage their use in a wide range of applications [1,2]

Cobalt zinc ferrite oxides are well known for the similarity of their chemical and physical properties, in relation with the electronic structures of transition metal cations. Despite this similarity, these oxides generally present diversified physical and chemical properties allowing their use in many applications from medicine (e.g.: MRI contrast agents, DNA isolation, magnetic and activated drug delivery) to electronics (e.g.: magnetostrictive and gas sensors, optoelectronics, microwave frequency devices, storage media) [3-4-5]. Nano-ferrites also show extraordinary properties as compared to the bulk material [6]. So, synthesizing nano-sized particles of spinel ferrites has recently attracted more attention of researchers due to the developments of technology and needs of society for functional materials with smaller size [7].

Due to fact-growing demands for the synthesis of various nanomaterials, the discovery of simple, quick, low cost and high efficient strategies has aroused many scientific efforts. Amongst nanomaterials, magnetic spinel ferrites, MFe_2O_4 (M: Metal; Co, Zn, Cu, Ni, Al,….), have been introduced as an important class of nanomaterials due to their magnetic, catalytic and opto-electrical properties [8]. The most of the described syntheses in literature show that the pure phase preparation of ferrites require a high temperature of calcination, severe experimental conditions and or complex equipment [9].

Fourier transform Infrared (FTIR) spectroscopy in the 500–4000 cm^{-1} range (mid-IR, 2.5 to 20 µm) is a direct probe of the molecular vibrations and interactions. FTIR absorption spectra of chemical compounds are often used to specifically identify structures and their activities. Over the last several years, technology upgrades have improved the performance of FTIR spectroscopy [10]. To our knowledge, several groups had exposed the

methane conversion monitored by FTIR technique in literature [11-12-13-14].
In the present study, we use FTIR spectroscopy to analyze gas conversion in presence of mixture of air-methane in order to test the reactivity of nanoparticles of $Co_{0.5}Zn_{0.5}Fe_2O_4$. Synthesis of nanoparticles of this materiel was carried out using a new technique based on coordination chemistry. For the first time, a strong reactivity of this product in presence of CH_4 in air was evidenced.

2. Experimental details

2.1. Synthesis method

$Co_{0.5}Zn_{0.5}Fe_2O_4$ nanoparticles were prepared by the method of co-precipitation, the chemical reagents used in this work were: $FeCl_2$, $4H_2O$, $Co(NO_3)_2$, $6H_2O$, ZnCl (All provided from *BiochemChemopharma*, purities ≥ 98 %). All reagents were of analytical grade and were used without further purification. All raw materials are mixed with deionized water individually, with addition of surfactant, using the following stoichiometric ratios (Molar Ratio (Cobalt; Zinc / Iron) = (0.5; 0.5/2) and Molar Ratio (surfactant/metal) = 0.5/1. The mixture was stirred until a clear solution was obtained. The precipitating agent NaOH (*Panreac*, 98 % assay) was added quickly to the mixture solution until obtaining a pH of suspension equal to 11. Then, the solution was heated to 70°C with constant stirring of 800 rpm for one hour. The precipitate was washed thoroughly with deionized water three times and then dried in an oven at a temperature of 100°C. The milled powder was heated in the furnace at a temperature of 700°C for 8 hours.

2.2. Characterizations

Phase identification was carried out using a Bruker diffractometer, D8 ADVANCED model, equipped with CuK_α radiation (λ=1.5406Å, voltage V=45kV, Intensity I=35mA). Modified Scherrer's formula [15] was used to estimate the mean crystallites size (D) of the samples using a corrected full-width at half-maximum value (β) obtained from the strongest peak. (see section 2.3), The lattice parameters were calculated using Powley and Le-Bail refinement methods.
The thermal decomposition in the air of the dried precursor was investigated using of differential thermal analysis (DTA) and thermogravimetric analysis (TGA), which were carried out in the temperature range of 25-1100°C with a TG-DTA 92 SETARAM with a heating rate of 10°C/min.
To determine the sample specific surface area (noted as A_{BET}), Brunauer–Emett-Teller (BET) [16] analyses were carried out making use of Quantachrome brand device. This method delivers the effective surface exposed to N_2 gas adsorption in m^2/g.
Thermogravimetric (TGA) and differential thermal (DTA) analysis of the dried precursor was carried out using SETARAM instrumentation up to 1000°C at a heating rate of 5°C min^{-1} in air atmosphere.

2.3. Phenomenon of the methane catalytic oxidation

without catalyst, the conversion of methane requires high temperatures, approaching to 1000 °C. Recall that the energy of the bond C-H is strong and hard to break (104 kcal/mol to 298 °K). For lowering the reaction temperature Many catalysts have been proposed [17,18].
In the presence of the catalyst, methane and oxygen are adsorbed separately to the heart of the material. The chemical adsorption of oxygen to the surface of the material leads to a transfer of the free electrons from the network to the adsorbed molecules, according to the following reactions:

- Molecular adsorption of oxygen: $O_2+e^- = O_2^-$
- Dissociative adsorption of oxygen: $O_2^-+ e^- = 2O^-$

When the material is exposed to gases other than oxygen present in the air, there may be a chemical reaction with the pre-adsorbed species, including oxygenated species. The reactions which take place are essentially redox reactions.

$$CH_4+2O_2 \rightarrow\rightarrow\rightarrow\rightarrow\rightarrow\rightarrow\rightarrow CO_2+2H_2O$$

2.4. Catalytic test and reactivity using FTIR spectroscopy

Figure 1 shows the experimental setup of the catalytic tests. The catalytic reactor was a cylindrical cell in which the sample can be exposed to reactive air-gas flows. The sample temperature was controlled by a thermocouple and stabilized at a given T_{react} value corresponding to a given reactivity. A fixed mass (m_0=0.1g for each test) of powder was placed between two porous (ZrO_2) separators. Blank experiments with these separators were systematically carried out to confirm the absence of activity in the cell itself. The gas flows (10 sccm), controlled by flowmeters (2500 ppm CH_4 in air), passed through separator 1, then the sample, and finally

separator 2, with a fixed slow speed of10 sccm. The reactor was heated in a furnace, at temperatures ranging between 175 and 525°C.

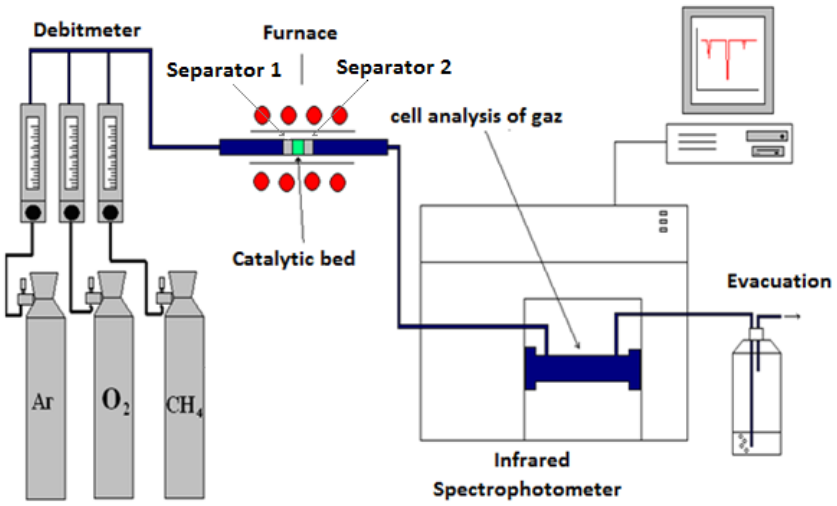

Figure 1: Catalytic setup used for testing catalytic conversion of CH_4

In this section, we study the reactivity of the sample in presence of air-CH_4 flows at various temperatures. The conversion reactions are revealed by the appearance of the infrared absorption band of CO_2 (doublet at 2340–2360 cm^{-1}), resulted from the following reaction:

$$CH_4+2O_2 \longrightarrow CO_2+2H_2O$$

The emitted gases were monitored by Fourier transform infrared (FTIR) spectrometer (*Bruker Vertex 70*). Blank experiments were performed to differentiate the CO_2 resulted from the ambiance. Each vibrational spectrum was recorded over a period of Δt = 10 s with intervals of 30 s between two spectra. The total exposure time was two hours.

The conversion intensity $I_{(CO2)}$ was determined from the measurements of CO_2 bands transmittance see the fig 2, at a certain time *t* of the gas/solid interaction. For a given total time *t* of reaction and a given temperature T_{react}, the intensity $I_{(CO2)}$ was defined as being proportional to the amount of CO_2 molecules formed during the time $\Delta t$of FTIR record. This value of $I_{(CO2)}$ expressed in arbitrary units (a.u.) depends on the total time *t* and on the temperature T_{react}. The FTIR intensities of CH_4 absorption peaks varied linearly with the air-gas composition. All experiments were characterized by a first initiating regime in which the CO_2 intensities increase up to a maximal value after a time of about 10-15 min.

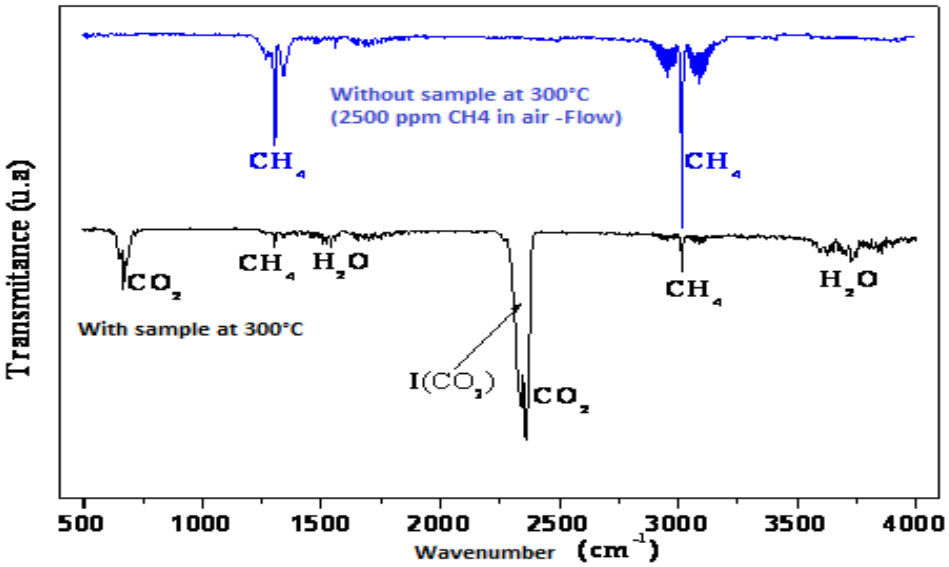

Figure 2: FTIR spectroscopy of emitted gases in the presence and absence of the CH_4catalyst

Figure 2 represents typical FTIR spectra associated with conversion of CH_4 after solid-gas interaction. The CO_2 FTIR band increases as the CH_4 band intensity decrease.
To compare various reactivities, we have normalized the curves $I_{(CO2)}$ by calculating the values $I^*_{(CO2)}=I_{(CO2)}/A_{BET}$. Let us recall that, as the sample masses are identical in all experiments, the A_{BET} values are directly proportional to the total surfaces of samples exposed to reactive gases.
It should be noted that in our experiments the temperature ranges were limited to 525°C for air-CH_4 flows in order to avoid direct oxidation of CH_4 by oxygen (this direct oxidation was tested in our experimental device in absence of active sample).

3. Results and Discussion

3.1. Thermal decomposition of precursor

Initially, the decomposition of the cobalt zinc ferrite precursor was investigated from thermogravimetry analyses. Figure 3 depicts the decomposition of ferrite precursor as a function of temperature. The thermal decomposition behavior of the precursor in air was followed up to ferrite formation. From this figure, it is clear that the weight loss starts at 23°C with the release of 1.5% up to 40°C attributed to the loss of water molecules. The second weight loss step sets on 165°C with a steep slope up to 307°C, exhibiting a weight loss of 1.2% agreed with the theoretically calculated loss due to the release of remaining water molecules from the precursor. The decomposition process of the formed anhydrous precursor is followed immediately after the dehydration process showing well-defined ATG step up to 385°C. These steps were attributed probably to the decomposition of ferrous, cobalt and zinc precursor. No loss of weight was observed after 700°C.

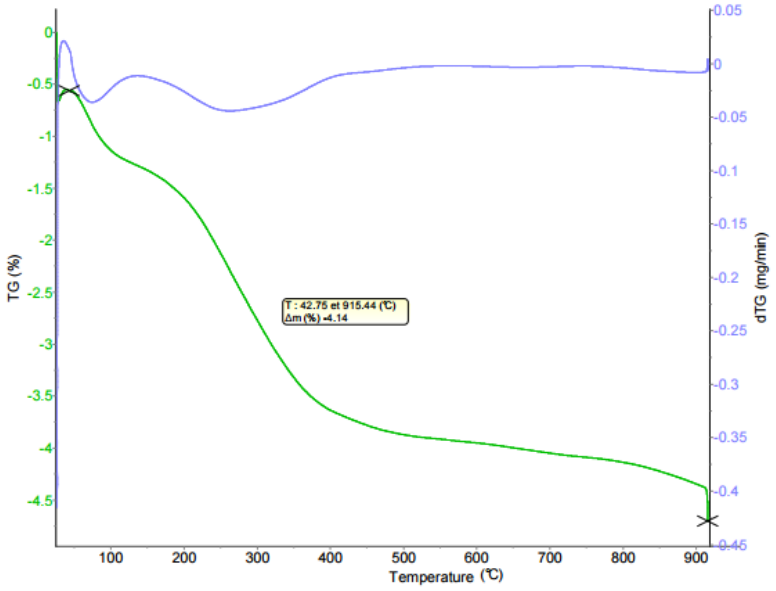

Figure 3: DTA-TG curves of ferrite $Co_{0.5}Zn_{0.5}Fe_2O_4$ precursor

3.2. X-ray diffraction Analysis

The crystal structure and phase purities of the synthesized sample were evaluated by powder X-ray diffraction (XRD). The XRD pattern of $Co_{0.5}Zn_{0.5}Fe_2O_4$ powder is shown in Figure 4. The most intense peaks indexed as (220), (311), (222), (400), (422), (333), and (440) are found well matched with single-phase cubic spinel (JCPDS Card no. 019-0629).
The average crystallites size for the synthesized powder is calculated using Scherrer's formula with respect to the high intense peak plane (311). The Scherrer's formula can be expressed as follows:

$$D = \frac{0.91 * \lambda}{\beta \cos\theta}$$

Here, λ is the wavelength of the $CuK_{\alpha 1}$ radiation and β is the full width at half maximum of the peak and θ the diffraction angle.

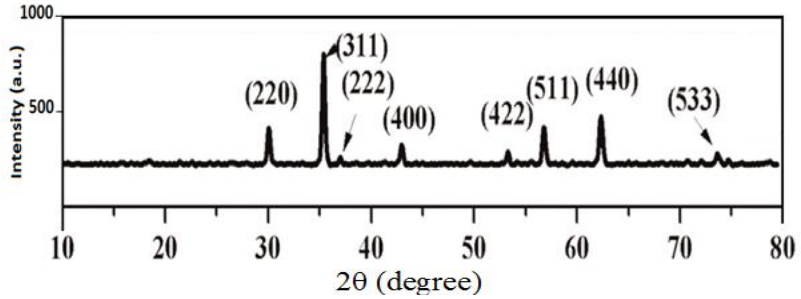

Figure 4: X- ray diffraction pattern of synthesized $Co_{0.5}Zn_{0.5}Fe_2O_4$

The various experimental cell parameters have been refined using PARAM software. Crystallites size (D) has been determined from X-ray diffraction profile. The various pertinent parameters (lattice parameters, mean crystallites size, the experimental BET specific surface area) are reported in table 1.

Table 1: Physical and chemical parameters obtained for $Co_{0.5}Zn_{0.5}Fe_2O_4$.

Item	**$Co_{0.5}Zn_{0.5}Fe_2O_4$**
Structural parameters	
Crystalline system	Cubic phase
Refined cell parameter (nm)	a = 8.397± 0.002
Scherrer size (nm)	17
BET specific surface area (m^2/g)	21.79
Average pore size (nm)	4.58

3.3. Atomic Force Microscopy scans

Figure 5 shows an overview of the sample using atomic force microscopy with the NAIOAFM Instrument (Nanosurf AG, Switzerland). It shows the topography view on the left and the phase view on the right. It is worth to note the presence of the islands up to 120 nm in altitude and one hundred nanometers in diameter. Line profile on two particles shows that the height of the islands was 35 nm. One could notice also the presence of small structures on the surface. The main observation is the filiforme of the synthesized powder. This clearly confirms the nanowires formation within our $Co_{0.5}Zn_{0.5}Fe_2O_4$ powders.

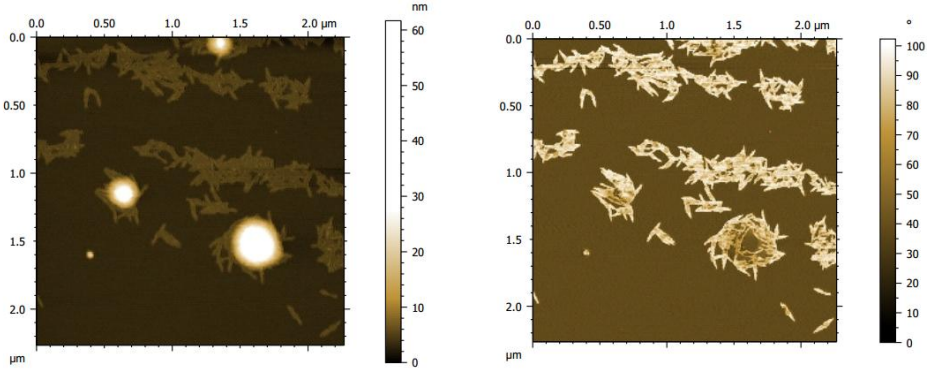

Figure 5:AFM images of the synthesized powder of $Co_{0.5}Zn_{0.5}Fe_2O_4$

3.4. Catalytic activity using FTIR Intensity

The figure 6 reports the normalized $I^*_{(CO2)}$ intensities with maximum values reached after 25 minutes of reaction for $Co_{0.5}Zn_{0.5}Fe_2O_4$sample reacting with air-CH_4, as a function of reaction time at various temperatures.

The reactivity of CH_4 with the ferrite (I* intensity as a function of time and temperature) starts at 200°C. It reaches a stabilization plateau after some minutes (20 to 25 minutes) depending on the temperature. Such an initiating period is systematically observed. It is due to a complex mechanism involving penetration of CH_4 gas into the polycrystalline wall, adsorption of molecules on grain surfaces, reaction of molecules with actives sites and regeneration of deactivated sites by air oxygen. More precisely, the maximum values of I^* result from a

competition between oxidation reaction of CH_4 molecules on active sites and oxidation of the reduced sites by oxygen molecules in the air.

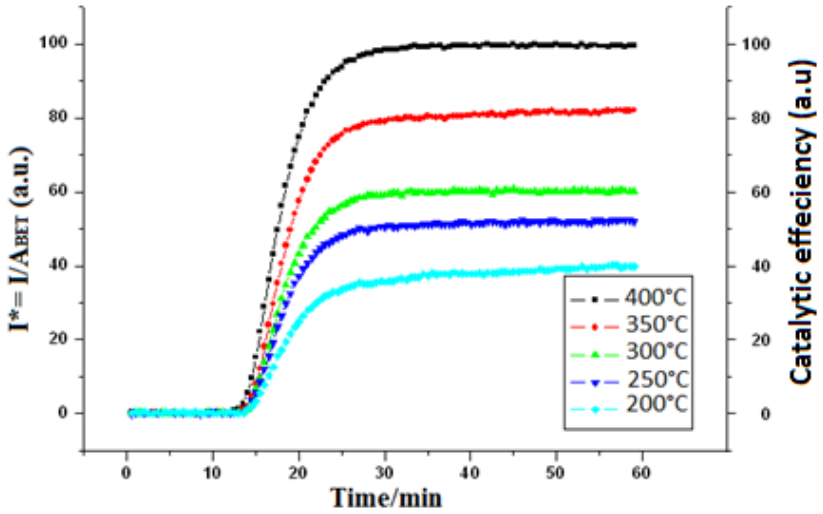

Figure 6: Normalized intensities $I^*_{(CO2)}$ for ferrite $Co_{0.5}Zn_{0.5}Fe_2O_4$ reacting with 2500 ppm of CH_4 in air as a function of reaction time at various temperatures

The evolution of maximum intensity I^* (corresponding to the stabilized I^* values) for $Co_{0.5}Zn_{0.5}Fe_2O_4$, reacting with air–CH_4, as a function of temperature, was reported in the figure 7. The activation energy (E_a) associated with these I^* values ($I^*=I_0\exp(-E_a/RT)$) may be deduced from this curve (E_a= 0.223 eV). All these experimental data (I^* values and activation energy) reveal that the polycrystalline sample $Co_{0.5}Zn_{0.5}Fe_2O_4$ has a high reactivity in presence of air - CH_4.

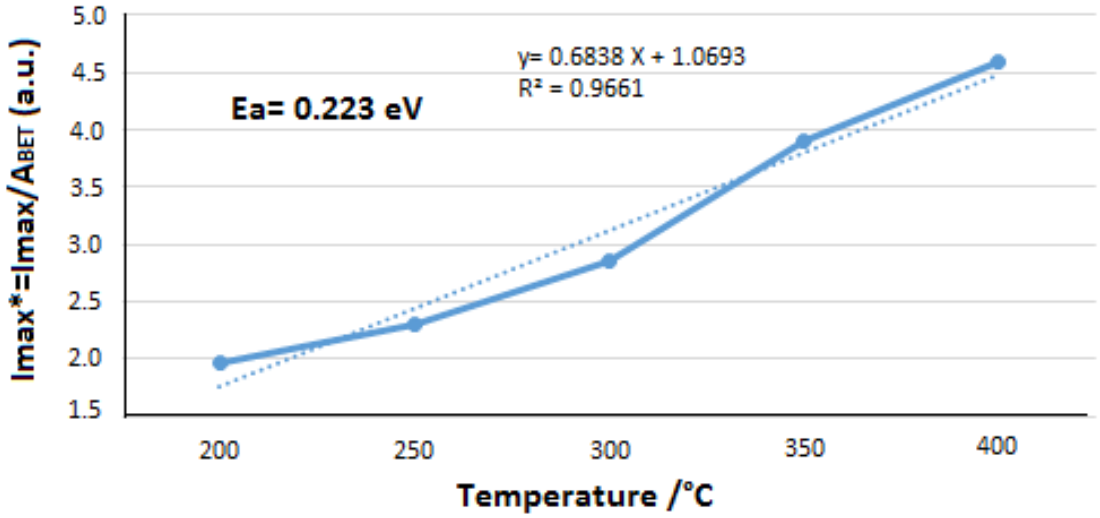

Figure 7: Evolution of maximum I^* values for $Co_{0.5}Zn_{0.5}Fe_2O_4$ reacting with 2500 ppm of CH_4 in air, as a function of the temperature. The activation energy value is reported

3.4. The catalytic effect of the ferrite

The catalysts containing noble metals hold an especially important attention because of their effectiveness [19]. The major drawback of these types of materials is their prohibitive costs. For this reason, many studies focus on the ferrite which has good catalytic activity with less expensive than noble metals.

The incorporation of cobalt in the crystal structure of the zinc ferrite generates the formation of gaps which improve the mobility and the diffusion of oxygen atoms within the catalyst. The adsorbed oxygen promotes the oxidation of the adsorbed species at the catalyst surface and decreases the amount of carbon deposited to prevent catalyst deactivation.

With these catalysts, carbon deposition is relatively low. It has little influence on the catalytic activity because the deposited carbon does not block the active sites.

Conclusion

Polycrystalline $Co_{0.5}Zn_{0.5}Fe_2O_4$was successfully synthesized at a moderate temperature. X-ray diffraction result confirms that the synthesized powder exhibits spinel cubic crystal structure with crystallites size of 17 nm. The high reactivity of ferrite $Co_{0.5}Zn_{0.5}Fe_2O_4$ polycrystalline phase in presence of air-CH_4 flows was a surprising result regarding the literature [20]. It should be noted that the synthesized ferrite powder was highly sensitive in presence of methane-air mixture. The reactivity starts at 200°C and reaches it maximum after 20 to 25 minutes depending on the temperature. The highest response was obtained at 400°C. All these results show clearly that this ferrite composition could be a promoting catalytically acting material for methane operating at modulated temperatures.

Acknowledgment

We gratefully acknowledge *Nanosurf AG*company (Switzerland) for taking measurement by their AFM instrument.

Conflict of Interest: The authors declare that they have no conflict of interest.

References

1. Bulai G., Diamandescu L., Dumitru I., Gurlui S., Feder M., Caltun O.F., *J. Magn. Magn. Mater.* 390 (2015) 123-131.
2. Parashar J., Saxena V.K., Jyoti, Deepak Bhatnagar D., Sharma K.B., *J. Magn. Magn. Mater.* 394 (2015) 105-110.
3. Liu F., Laurent S., Roch A., Vander Elst L., Muller R.N., *J. Nanomater.* Volume 2013 (2013), Article ID 462540.
4. Španová A., Rittich B., Beneš M.J., Horák D., *J. Chromatogr. A.* 1080 (2005) 93-98.
5. Amiri S., Shokrollahi H., Mater. Sci. Eng. 33 (2013) 1-8**.**
6. Hassan A., Khan M. A., Shahid M., Asghar M., Shakir I., Naseem S., Riaz S., Warsi M. F., *J. Magn. Magn.Mater.* 393 (2015) 56-61.
7. Hajalilou A., Hashim M., Masoudi M. T., *Ceram. Int.* 41 (2015) 8070-8079.
8. Tadjarodi A., Salehi M., Imani M., *Mater. Lett.* 152 (2015) 57-59.
9. Bo X., LiG., Qiu X., Xue Y., Li L., *J. Solid. State. Chem.* 180 (2007) 1038-1044.
10. Peri J. B., *in. Catal. : Sci. Technol.*, ed. By Anderson J. R., Boudart M. 5 (1984) 171-220.
11. Favre A. , Guilhaume N. , Millet J.-M. M., Primet M., *Catal. Lett.* 49 (1997) 207-211.
12. Kaddouri A. H., De Blasio N., Del Rosso R., React. Kinet. *Catal. Lett.* 72 (2001) 309-320.
13. dos Santos A. G., Arab M., Patout L., de Souza C. P., *Catal.* 4 (2014) 77-88.
14. Ajroudi L., Villain S., Madigou V., Mliki N., Leroux C., *J. Cryst. Growth.* 312 (2010) 2465-2471.
15. Gabal M.A., AlAngari Y.M., *Mater. Chem. Phys.* 118 (2009) 153-160.
16. Brunauer S., Emmett P.H., Teller E., *J. Am. Chem. Soc.* 60 (1938) 309-319.
17. Fathi M., Monnet F., Schuurman Y., Holmen A., Mirodatos C., *J. Catal.* 190 (2000) 439-445.
18. Mattos L.V., de Oliveira E.R., Resende P.D., Noronha F.B., Passos F.B., *Catal. Today.* 77 (2002) 245-256.
19. Au C.T., Wang H.Y., *J. Catal.* 167 (1997) 337-345.
20. Nowakowski P., Villain S., Kopia A., Suliga I., Gavarri J. R., *Appl. Surf. Sci.* 254 (2008) 5675-5682.